79-4057

Horizontal Buoyancy Effects on the Pressure Distribution of a Body in a Duct

Gerald C. Lauchle*
Applied Research Laboratory, The Pennsylvania State University, State College, Pa.

It is well known that the static pressure coefficient values obtained from tests of axisymmetric bodies in, for example, a large water tunnel indicate the existence of tunnel wall interference. This interference is due to blockage experienced by the body operating within the boundaries of the test section walls, and to the skin friction on both the tunnel walls and the surface of the body which, in turn, causes finite thickness boundary layers to develop. These factors result in a decrease in static pressure along the test section which leads to a spurious horizontal buoyancy on the body. Potential flow calculations can only account for solid blockage effects. A control volume analysis has thus been carried out from which pressure coefficient correction terms due to horizontal buoyancy have been obtained. The present method permits one to treat relatively large bodies which have a much stronger interaction with the tunnel walls. These correction factors are computed for a large, streamlined body operating over a range of velocities in The Pennsylvania State University, Garfield Thomas 1.22-m diam water tunnel. They are applied to a theoretically determined potential flow in-tunnel body pressure distribution to obtain the viscous flow pressure distributions which are compared to those determined experimentally. The agreement between theory and experiment is shown to be very good over all speeds considered.

Nomenclature

A = blocked area between the body and duct wall
A_e = effective area between the body and duct wall, including displacement thickness effect
A_o = area of duct
a = numerical constant in Eq. (38)
B_i = continuity integral, Eqs. (32) and (33)
C_o = numerical constant in Eq. (38)
Cp = pressure coefficient
ΔCp = pressure coefficient correction
ΔCp_i = components of ΔCp ($i=1,2,...$)
ΔCp_{II} = ΔCp_I for laminar body flow
ΔCp_{I2} = ΔCp_I for turbulent body flow
$D_{\max}$ = maximum diameter of the body
d_o = distance from nose of body to geometrical beginning of the water tunnel test section
F_i = fluid forces ($i=1,2,...$)
I_i = momentum integral, Eqs. (29) and (30)
K_n = body fineness ratio ($l_n/D_{\max}$)
k = numerical constant in Eq. (38)
L = total body length
l = duct length used in potential flow calculation
l_o = distance from nose of body to point on duct wall where turbulent boundary layer begins
l_n = distance from nose to $D_{\max}$
P_o = freestream static pressure
p = local fluid pressure
p_b = pressure exerted by the body on the fluid
p_b' = "displaced body" pressure exerted by the body on the fluid
R_L = radius of curvature of the body tailcone
Re_L = body-length Reynolds number
r = radius coordinate
s = arc length coordinate
s_t = transition arc length
U_∞ = freestream velocity in duct far upstream of the body
u = local fluid velocity
u_i = velocity profile for body ($i=1$, laminar; $i=2$, turbulent)
u_o = reference velocity in potential flow computation
u_r = numerical rake output far upstream of the body (U_∞/u_0)
u_{rp} = numerical rake output near the body at, for example, a pitot probe location
x = axial coordinate where origin is l_0 upstream from nose of the body
$\bar{x}$ = body axial coordinate ($x-l_0$)
$\hat{x}$ = nondimensional body axial coordinate ($\bar{x}/l_n$)
x' = dummy variable of integration
$\hat{y}$ = nondimensional body radius ($r_b/D_{\max}/2$)
δ = boundary-layer thickness
δ_i = body boundary-layer thickness ($i=1$, laminar; $i=2$, turbulent)
δ^* = boundary-layer displacement thickness
ϵ_L = expression given by Eq. (39)
ν = kinematic viscosity
ρ = fluid mass density
τ = wall shear stress
ϕ = angle formed between tangent line of body and the x axis

Subscripts

b = body
E = experimental
I = inviscid
m = measured
V = viscous
w = duct wall

Received Aug. 28, 1978; revision received Dec 7, 1978.

Index categories: Hydrodynamics; Nozzle and Channel Flow.

*Research Associate.

Introduction

THE investigation of flows about bodies of revolution in cylindrical ducts is of general interest to those concerned with turbomachinery, wind-tunnel, and water-tunnel testing to note a few. There have been several methods proposed for the determination of the potential flow about bodies operated within ducts of both constant and nonuniform cross section.[1-5] These methods allow for blockage effects due to the duct (or test section walls). However, these methods do

not allow for viscous effects that occur on the body and tunnel walls. Viscosity gives rise to skin friction on all surfaces in contact with the flowing fluid which, in turn, gives rise to boundary-layer growth. The displacement thickness varies from the beginning of boundary-layer growth to distant points far downstream, effectively changing the cross-sectional areas of both the body and the duct. This added constriction of the flow and the skin friction creates a second type of blockage characterized by a static pressure drop from the beginning of boundary-layer growth to any arbitrary point downstream. This net change in static pressure may be interpreted in the form of a force in the horizontal direction (assuming the tunnel test section is horizontal), which is the so-called "horizontal buoyancy."

In many applications, it is necessary to know as precisely as possible, the pressure distribution on a particular body operating in a given tunnel test section. Because of horizontal buoyancy effects, a typical inviscid flow calculation will not yield totally accurate results for large diameter bodies (relative to the diameter of the test section). This statement may be verified through a direct comparison of experimentally determined pressure distributions with a potential flow prediction. Figure 1 shows such a comparison. The axisymmetric body here is 3.05 m long and has a maximum diameter of 32.39 cm. The pressure coefficient data were obtained on this body while it operated in the Garfield Thomas 48-in. (1.22 m) diam water tunnel located at the Applied Research Laboratory of The Pennsylvania State University. A description of the experiments will be presented in a later section. The potential flow calculation shown in Fig. 1 was performed using the "Douglas-Neumann code."[1,2] Solid blockage due to the 1.22 m diam test section is included in this computation. The experimental pressure coefficients are seen to be lower than those predicted at a given point on the body and are velocity dependent. This discrepancy is ascribed to horizontal buoyancy.

Measurements of body pressure distributions are not economically practical in all cases. The next best alternative, therefore, is to approach analytically the problem of horizontal buoyancy. This paper presents such an analysis where correction terms are derived that may be applied to the results of a given potential flow calculation. As examples of the analysis, we include calculations for the body of Fig. 1 and compare them with the experimentally determined data. Although the analysis given here is for axisymmetric bodies operating in cylindrical test sections of constant radius, it is quite general so that its adaptation to other configurations (variable-radius test sections, for example) would seem straightforward.

Analysis

Potential Flow Considerations

The potential flow pressure distribution on an arbitrarily shaped axisymmetric body operating within the confines of a cylindrical duct of a circular cross section may be calculated using the Douglas-Neumann computer code,[1,2] among others.[3-5] A typical computation with the Douglas-Neumann code might use the modeling shown in Fig. 2a. Because of the limited core size in our digital computers, the length of the duct (which is described by discrete points) must be finite when using this method. If the duct is assumed to extend from $\bar{x}=-l$ to $\bar{x}=l+L$, where L is the body length, then the resulting pressure coefficient values on the body (Cp) are normalized to an unspecified reference velocity, u_0. We know, however, that in the limit $l\to\infty$, $u_0\to U_\infty$ (U_∞ is the true velocity at infinity). Consequently, in conjunction with our computation of the potential flow about the body, we also determine $u_r \equiv U_\infty/u_0$ at $\bar{x}=-l$, where l is assumed much larger than L. Knowing u_r, the calculated pressure coefficient values may then be corrected to the reference velocity U_∞ by a simple computation:

$$Cp_l = 1-(u_l/u_0)^2(u_0/u_\infty)^2$$
$$= 1-(1-Cp)/u_r^2 \tag{1}$$

where Cp_l represents the potential flow pressure coefficient on a body operating in a cylindrical tube of infinite extent. Equation (1) is most useful to use when a number of pressure distributions are to be calculated for a family of bodies and compared; it assures a consistent reference velocity.

By defining a control volume from Fig. 2a to extend from $\bar{x}=-\infty$ to an arbitrary $\bar{x}$ on the body, the continuity equation may be written as:

$$A_o U_\infty = A u_l \tag{2}$$

where

$$A_o = \pi r_w^2 \tag{3}$$

$$A = \pi(r_w^2 - r_b^2) \tag{4}$$

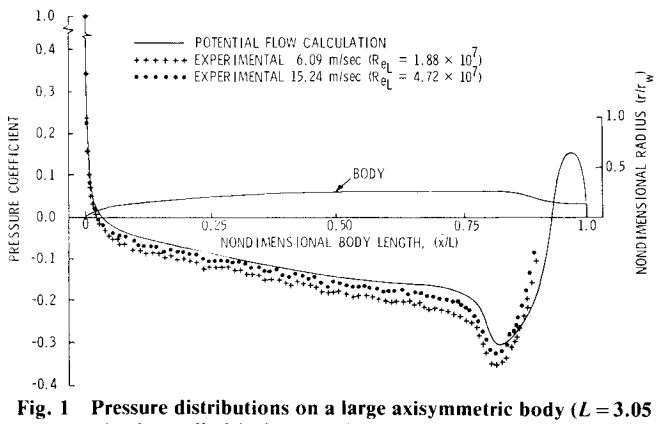

Fig. 1 Pressure distributions on a large axisymmetric body ($L=3.05$ m) operating in a cylindrical test section ($r_w=1.22$ m).

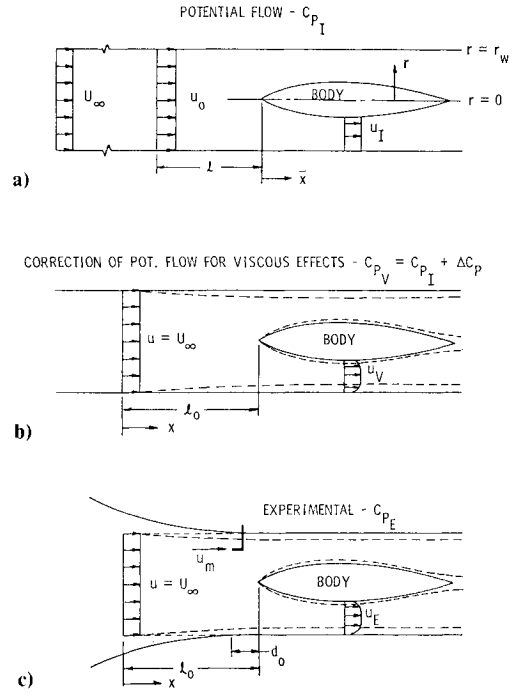

Fig. 2 a) Potential flow over a body in an infinitely long cylindrical duct; b) a schematic description of boundary-layer buildup on the body and duct wall depicting that u_V is different from u_I; and c) a schematic description of the flow over a body in an experimental situation.

with r_w and r_b being the tunnel wall and body radii, respectively. We may also write the momentum flux equation:

$$\rho u_1^2 A - \rho U_\infty^2 A_o = F_1 + F_2 + F_3 \tag{5}$$

where ρ is the density of the fluid and the F_i's ($i=1,2,3$) are the forces acting on the control volume. Assuming positive forces to act in the positive $\bar{x}$ direction, we have

$$F_1 = P_o A_o \tag{6}$$

and

$$F_2 = -p_1 A \tag{7}$$

where P_0 is the freestream static pressure and p_1 is the potential pressure that occurs in the fluid at any arbitrary location within the control volume. The third force, F_3, is due to the pressure exerted by the body in the $\bar{x}$ direction. It depends, therefore, on the pressure distribution of the body, $p_b(\bar{x})$. The differential form of this force may be written as:

$$dF_3 = -p_b \sin\phi \, dA_b \tag{8}$$

where ϕ is the angle between the tangent line of the body at point $\bar{x}$ and the $\bar{x}$ axis and

$$dA_b = 2\pi r_b ds = 2\pi r_b d\bar{x}/\cos\phi \tag{9}$$

where s is the arc-length coordinate. We can integrate dF_3 along the body and get

$$F_3 = -2\pi \int_0^{\bar{x}} p_b r_b \tan\phi \, dx' \tag{10}$$

We may now solve Eq. (5) for p_1 (contained in F_2) and use Eq. (2) to obtain:

$$p_1 = P_o \frac{A_o}{A} - \rho U_\infty^2 \frac{A_o^2}{A^2} + \rho U_\infty^2 \frac{A_o}{A} - \frac{2\pi}{A} \int_0^{\bar{x}} p_b r_b \tan\phi \, dx' \tag{11}$$

This equation describes the inviscid pressure that occurs in the fluid at location $\bar{x}$ ($0 \le \bar{x} \le L$). We will now derive the corresponding equation for this pressure when viscous effects are included.

Viscous Flow Considerations

Viscosity gives rise to wall shear stress and boundary-layer development on both the body and the tunnel wall. A new control volume must be considered which is shown in Fig. 2b. We choose the beginning of this control volume to be a distance l_0 upstream of the forward stagnation point of the body, where the new axial coordinate $x = \bar{x} + l_0 = 0$. This origin is judiciously selected to be the point where a turbulent boundary layer begins to form on the tunnel wall. We will further assume that l_0 is large enough relative to the body length such that the velocity is uniform across the duct at $x = 0$. Without any loss of generality, we call this velocity U_∞.

The general form of the continuity equation for the control volume of Fig. 2b is:

$$A_o U_\infty = 2\pi \int_{r_b}^{r_w} u r dr \tag{12}$$

where u is the nonuniform velocity profile between the body and tunnel wall. In like manner, we can write the change in momentum flux as:

$$2\pi\rho \int_{r_b}^{r_w} u^2 r dr - \rho U_\infty^2 A_o = \sum_{i=4}^{8} F_i \tag{13}$$

where

$$F_4 = P_0 A_0 \quad F_5 = -P_V A \quad F_6 = -2\pi \int_{l_0}^{x} p_b' r_b \tan\phi \, dx'$$

$$F_7 = -2\pi \int_{l_0}^{x} r_b \tau_b dx' \quad F_8 = -2\pi r_w \int_0^x \tau_w dx'$$

The quantity p_V is the viscous pressure that occurs in the fluid between the body and tunnel wall at location x, and p_b' is the displaced-body pressure, i.e., it is a perturbed p_b due to the added spatial acceleration of the flow caused by the body boundary-layer development. It may be calculated using potential flow methods, but with the body radius redefined by $r_b' = r_b + \delta_b^*$, where δ_b^* is the body boundary-layer displacement thickness. The quantities τ_b and τ_w are the wall shear stresses that occur on the body and tunnel wall, respectively. It is noted that F_7 does not contain a $\cos\phi$ term because F_7, by assumption, is the x component of the force due to body wall shear stress. Equation (13) can be readily solved for p_V to obtain an analogous form of Eq. (11) for viscous flow.

Pressure Coefficient Correction

To obtain a viscous flow correction for the in-tunnel, inviscid pressure coefficient Cp_1, we form the difference

$$p_V - p_1 = \rho U_\infty^2 \frac{A_0^2}{A^2} + \frac{2\pi}{A} \left\{ \int_{l_0}^{x} p_b r_b \tan\phi \, dx' - \int_{l_0}^{x} p_b' r_b \tan\phi \, dx' \right.$$

$$\left. - \int_{l_0}^{x} r_b \tau_b dx' - r_w \int_0^x \tau_w dx' - \rho \int_{r_b}^{r_w} u^2 r dr \right\} \tag{14}$$

where the change of variable $x = \bar{x} + l_0$ was made in Eq. (11).

A pressure coefficient correction term may be defined by:

$$\Delta Cp = Cp_V - Cp_1 = p_V - p_1 / \tfrac{1}{2}\rho U_\infty^2 \tag{15}$$

It is convenient to express ΔCp as the sum of individual terms, i.e.,

$$\Delta Cp = \sum_{i=1}^{4} \Delta Cp_i \tag{16}$$

where

$$\Delta Cp_1 = 2\frac{A_0^2}{A^2} - \frac{4\pi}{A U_\infty^2} \int_{r_b}^{r_w} u^2 r dr \tag{17}$$

$$\Delta Cp_2 = -\frac{4\pi}{A\rho U_\infty^2} \int_{l_0}^{x} r_b \tau_b dx' \tag{18}$$

$$\Delta Cp_3 = -\frac{4\pi r_w}{A\rho U_\infty^2} \int_0^x \tau_w dx' \tag{19}$$

and

$$\Delta Cp_4 = \frac{4\pi}{A\rho U_\infty^2} \left\{ \int_{l_0}^{x} p_b r_b \tan\phi \, dx' - \int_{l_0}^{x} p_b' \tan\phi \, dx' \right\} \tag{20}$$

Under the assumption that a turbulent boundary layer originates at $x = 0$ and that $(l_0 + L) \le 10 r_w$, then the wall shear stress, τ_w, can be calculated from flat-plate expressions.[6,7] After making the substitution[6]

$$\tau_w = 0.0225 \, \rho U_\infty^2 (\nu / U_\infty \delta_w)^{1/4} \tag{21}$$

into Eq. (19), where the boundary-layer thickness is given by

$$\delta_w = 0.37 x (U_\infty x / \nu)^{-1/5} \tag{22}$$

Evaluation of the integral in Eq. (19) follows. It is found that

$$\Delta Cp_3 = -0.144\pi r_w (\nu/U_\infty)^{1/5} x^{4/5}/A$$
$$5\times 10^5 < U_\infty x/\nu < 10^7 \tag{23}$$

where ν is the kinematic viscosity and $A = A_0$ for $x \le l_0$. For arbitrarily shaped bodies, the integrals of Eqs. (18) and (20) must be evaluated numerically.

The integral in Eq. (17), however, may be evaluated in closed form if certain assumptions are made regarding the velocity profile $u(r)$. Clearly,

$$I_i \equiv \int_{r_b}^{r_w} u^2 r dr = \int_{r_b}^{r_b+\delta_i} u_i^2 r dr + u_V^2 \int_{r_b+\delta_i}^{r_w-\delta_w} r dr + \int_{r_w-\delta_w}^{r_w} u_w^2 r dr \tag{24}$$

where subscript i equals 1 for laminar body flow and is equal to 2 for turbulent body flow. The boundary-layer velocity profile, u_w, at the tunnel wall is (as just noted) assumed turbulent, i.e.,[6]

$$u_w = u_V [(r_w - r)/\delta_w]^{1/7} \tag{25}$$

On the turbulent flow body,

$$u_2 = u_V [(r - r_b)/\delta_2]^{1/7} \tag{26}$$

where δ_2 is of the same analytical form as Eq. (22), but with x being replaced by the arc-length coordinate s. For the case of a laminar-flow body, we assume a sine function velocity profile which, according to Schlichting,[6] very accurately approximates the exact Blasius profile. Thus, assuming

$$u_1 = u_V \sin[\pi (r - r_b)/2\delta_1] \tag{27}$$

with

$$\delta_1 = 4.7953 (\nu s/U_\infty)^{1/2} \tag{28}$$

Eq. (24) can be integrated. Omitting details,

$$I_1 = u_V^2 \left\{ \left(\frac{4-\pi^2}{4\pi^2}\right)\delta_1^2 - \frac{r_b\delta_1}{2} + \frac{\delta_w^2}{16} - \frac{2}{9} r_w \delta_w + \frac{A}{2\pi} \right\} \tag{29}$$

for laminar flow on the body and

$$I_2 = u_V^2 \left\{ -\frac{\delta_2^2}{16} - \frac{2}{9} r_b \delta_2 + \frac{\delta_w^2}{16} - \frac{2}{9} r_w \delta_w \frac{A}{2\pi} \right\} \tag{30}$$

for turbulent flow on the body.

In order to eliminate u_V^2 from I_i, Eq. (12) must be integrated. Again, we write

$$B_i \equiv \int_{r_b}^{r_w} u r dr = \int_{r_b}^{r_b+\delta_i} u_i r dr + u_V \int_{r_b+\delta_i}^{r_w-\delta_w} r dr + \int_{r_w-\delta_w}^{r_w} u_w r dr \tag{31}$$

finding

$$B_1 = u_V \left\{ \left(\frac{8-\pi^2}{2\pi^2}\right)\delta_1^2 + \left(\frac{2-\pi}{\pi}\right) r_b \delta_1 + \frac{\delta_w^2}{30} - \frac{r_w\delta_w}{8} + \frac{A}{2\pi} \right\} \tag{32}$$

and

$$B_2 = u_V \left\{ \left(\frac{\delta_w^2 - \delta_2^2}{30}\right) - \left(\frac{r_w\delta_w + r_b\delta_b}{8}\right) + \frac{A}{2\pi} \right\} \tag{33}$$

Because $B_i = A_o U_\infty / 2\pi$, we obtain

$$u_V = A_o U_\infty \left\{ A - \left(\frac{8-\pi^2}{\pi}\right)\delta_1^2 + 2(2-\pi) r_b \delta_1 - \frac{\pi r_w \delta_w}{4} + \frac{\pi}{15}\delta_w^2 \right\}^{-1} \tag{34}$$

for $i = 1$ (laminar flow) and

$$u_V = A_o U_\infty \left\{ A - \frac{\pi}{4}(r_b\delta_2 + r_w\delta_w) + \frac{\pi}{15}(\delta_w^2 - \delta_2^2) \right\}^{-1} \tag{35}$$

for $i = 2$ (turbulent flow).

The first term of ΔCp may be expressed in the form $\Delta Cp_I = \Delta Cp_{Ii}$ ($i = 1$ or 2). For laminar flow on the body, we find:

$$\Delta Cp_{11} = 2\frac{A_o^2}{A^2} - \frac{2A_o^2\left\{A + \left(\frac{4-\pi^2}{2\pi}\right)\delta_1^2 - \pi r_b\delta_1 - \frac{4\pi r_w\delta_w}{9} + \frac{\pi\delta_w^2}{8}\right\}}{A\left\{A - \left(\frac{8-\pi^2}{\pi}\right)\delta_1^2 + 2(2-\pi) r_b\delta_1 - \frac{\pi r_w\delta_w}{4} + \frac{\pi}{15}\delta_w^2\right\}^2} \tag{36}$$

For turbulent flow on the body, we find:

$$\Delta Cp_{12} = 2\frac{A_o^2}{A^2} - \frac{2A_o^2\left\{A - \frac{4\pi}{9}(r_w\delta_w + r_b\delta_2) + \frac{\pi}{8}(\delta_w^2 - \delta_2^2)\right\}}{A\left\{A - \frac{\pi}{4}(r_w\delta_w + r_b\delta_2) + \frac{\pi}{15}(\delta_w^2 - \delta_2^2)\right\}^2} \tag{37}$$

If the boundary layers are thin, one may, of course, neglect the higher order terms in δ_w and δ_i.

Application of the Theory

Body Shape

Based on the preceding analysis, computations have been performed for a large, streamlined body designed to operate in the Garfield Thomas 1.22-m diam water tunnel.[8] This body is described mathematically by:

$$\hat{y} = \sqrt{\hat{x}(2-\hat{x})} - K_n \frac{C_0 \hat{x}}{2a^2} \exp\left\{ -\frac{\hat{x}^2}{2a^2} - kK_n \right\} + \hat{x}^2 \epsilon_L \tag{38}$$

where $\hat{x} = x/l_n$, l_n = nose length, $\hat{y} = r_b/D_{\max}/2$, $D_{\max}$ = maximum diameter of the body, $K_n = l_n/D_{\max}$, and a, C_0, and k are numerical constants. The parameter

$$\epsilon_L = \frac{K_n C_o}{2a^2} \exp\left\{ -\frac{1}{2a^2} - kK_n \right\} \tag{39}$$

The tailcone is formed by an 18 deg arc of radius

$$R_L = \frac{2.5 D_{\max}}{2\sin 18\text{deg}} \tag{40}$$

An inflection curve is then faired between the end of the arc (at $\phi = 90 - 18 = 72$ deg) and a 4-in. diam disk whose center is coincident with the axis of symmetry. This body shape is shown in Fig. 1 for $a = 0.3$, $C_0 = 0.0303$, and $k = 0.45227$. The total length, L, is 3.05 m and $D_{\max}$ is 32.39 cm.

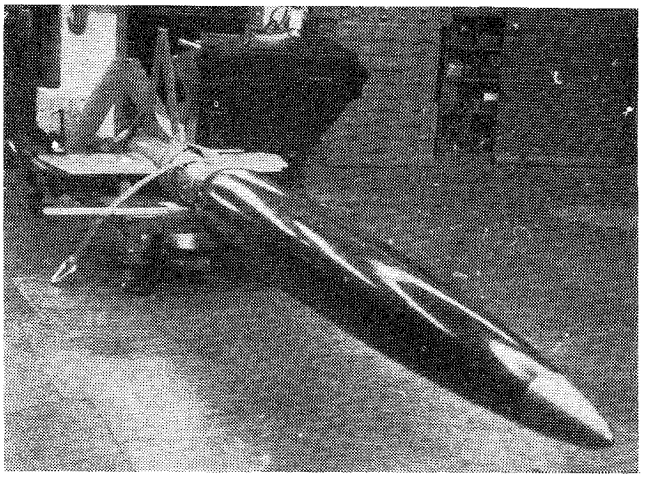

Fig. 3 Body used in the experimental portion of this investigation.

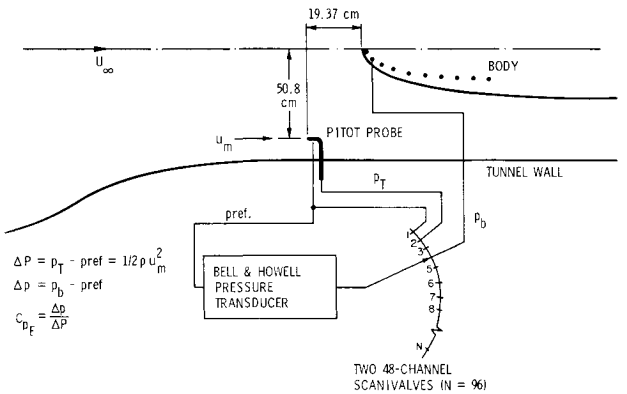

Fig. 4 Schematic of the data acquisition and reduction requirements used to obtain the experimental pressure distributions.

Experimental Pressure Distributions

The experimental body was manufactured by building up multiple layers of fiberglass cloth and resin. A precision template was used to form the body to final shape before the last coating of resin fully hardened. Figure 3 shows a photograph of the completed body and sting mount used to hold it in the 1.22-m diam test section. A total of 94 pressure taps of 0.79 mm in diameter were located in the surface of the body. Each body tap was connected to a flexible plastic tube which passed through the inside of the body, through the sting, and out of the tunnel. The 94 tubes then connected to two 48-channel Scanivalves and a single Bell and Howell calibrated pressure transducer. Before all runs, the tubes were bled to remove air pockets. Figure 4 shows a schematic of the experimental arrangement and the equations used in data reduction to obtain Cp_E.

As indicated in Figs. 2c and 4, the reference velocity in the measurements u_m was obtained with a pitot probe placed relatively close to the body and tunnel wall. Consequently, u_m may not be interpreted as the U_∞ used in the theoretical analysis. The velocity u_m differs from U_∞ because of both potential effects induced by the body and viscous effects created by tunnel wall boundary-layer growth.

Detailed measurements of the turbulent boundary-layer growth on the wall of the Garfield Thomas water tunnel were performed and reported by Ross, et al.[7] They concluded that an effective origin for the start of boundary-layer growth is 1.5 r_w upstream from the geometric beginning of the test section. That is, one may assume that the cylindrical test section can be fictitiously extended upstream into the settling section a distance 1.5 r_w and refer to this point as the entrance of the test section, Fig. 2c. Thus, we can assume $l_o = 1.5 r_w + d_o$, where d_o is the distance from the nose of the body to the actual beginning of the cylindical test section ($d_o = 54.6$ cm in this arrangement).

In order to compare experimental and theoretical pressure distributions, it is apparent that Cp_E (referenced to u_m) must be corrected in order to account for the differences between u_m and U_∞. This is done in two steps.

First, Cp_E is corrected for the tunnel wall boundary-layer displacement thickness at the position of the pitot probe. This thickness varies from 2.02 mm at 15.24 m/s to 2.42 mm at 6.09 m/s (the range of velocities considered in this investigation). The pitot probe was 10.16 cm from the wall and, thus, was out of the boundary layer. The effective area of the tunnel at the position of the pitot probe is:

$$A_e = A_o - 2\pi r_w \delta_w^* + \pi \delta_w^2 \simeq A_o - 2\pi r_w \delta_w^* \tag{41}$$

From the continuity equation [Eq. (12)], we can write

$$(u_m/U_\infty)_v = A_o/A_e \tag{42}$$

which represents the increase in u_m relative to U_∞ due to boundary-layer growth. The experimental pressure coefficient corrected to U_∞ only by viscous considerations is thus:

$$Cp_E^V = 1 - (u_E/u_m)^2 (u_m/U_\infty)_V^2 = 1 - (1 - Cp_E)(A_o/A_e)^2 \tag{43}$$

We know, because of the close proximity of the pitot probe to the body, that u_m may also be influenced by the potential effects of the body. In order to correct for this, a potential flow solution (Douglas-Neumann code) is used to calculate the velocity ratio $u_{rp} = U_\infty/u_m$ at the pitot probe location. Then,

$$Cp_E^{cor.} = 1 - (1 - Cp_E^V)/u_{rp}^2 \tag{44}$$

is the final correction of Cp_E. Furthermore, it makes no difference which correction is applied first. For the experimental arrangement used here, we found $u_{rp} = 0.9976$, and that A_o/A_e ranges from 1.013 to 1.016.

The experimental pressure distributions shown in Fig. 1 have been corrected according to the preceding discussion.

Results

The generality of the preceding analysis allows both laminar and turbulent body flow. As part of the experimental program, we, therefore, measured the laminar-to-turbulent transition points at the four tunnel velocities in which pressure distributions were measured. A wedge-shaped hot-film probe and anemometer system were used in these measurements. Table 1 summarizes the transition location results. For those body coordinates forward of s_t (transition arc length), the laminar form of the pressure coefficient correction analysis is used [Eq. (36)] and, τ_b in Eq. (18) is calculated according to the formula

$$\tau_b = 0.332\, \rho \nu U_\infty (U_\infty/\nu s)^{1/2} \tag{45}$$

Table 1 Experimentally determined transition points on the body used in the pressure distribution measurements

Tunnel velocity, U_∞ (m/s)	Body-length Reynolds No., $Re_L = U_\infty L/\nu$	Transition point, s_t/L	Transition Reynolds No., $Re_L (s_t/L)$
6.09	1.88×10^7	0.150	2.82×10^6
9.14	2.83×10^7	0.116	3.28×10^6
12.19	3.76×10^7	0.100	3.76×10^6
15.24	4.72×10^7	0.083	3.93×10^6

Table 2 Typical values for ΔCp_i ($i=1,2,3,4$) at 6.09 m/s, the inviscid pressure coefficient, and the corrected inviscid pressure coefficient for horizontal buoyancy effects

Body coordinate, $\bar{x}/L=(x-l_0)/L$	ΔCp_1	ΔCp_2	ΔCp_3	ΔCp_4	$\Delta Cp=\sum_{i=1}^{4}\Delta Cp_i$	Cp_I	Cp_V
0.002	−0.0038	0.000	−0.0139	0.00009	−0.0177	+0.433	+0.415
0.075	−0.0046	−0.00003	−0.0158	0.00047	−0.0199	−0.036	−0.056
0.253	−0.0065	−0.0006	−0.0202	0.00061	−0.0267	−0.087	−0.113
0.497	−0.0091	−0.0020	−0.0261	0.00069	−0.0366	−0.139	−0.176
0.667	−0.0108	−0.0031	−0.0300	0.00071	−0.0432	−0.161	−0.204

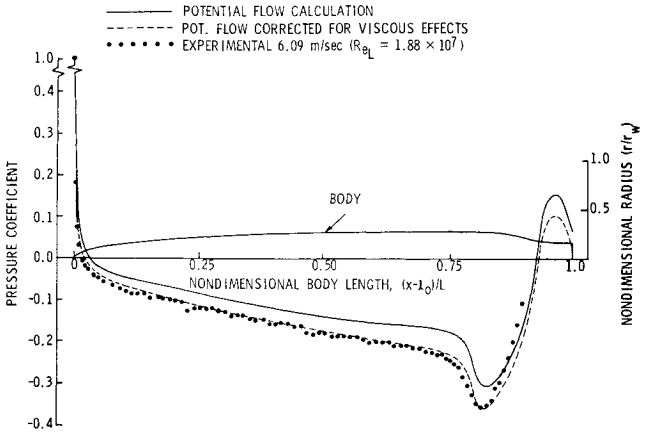

Fig. 5 Comparison of the in-tunnel potential flow and corrected potential flow pressure distributions with one determined experimentally at 6.09 m/s in the 1.22-m-diam water tunnel.

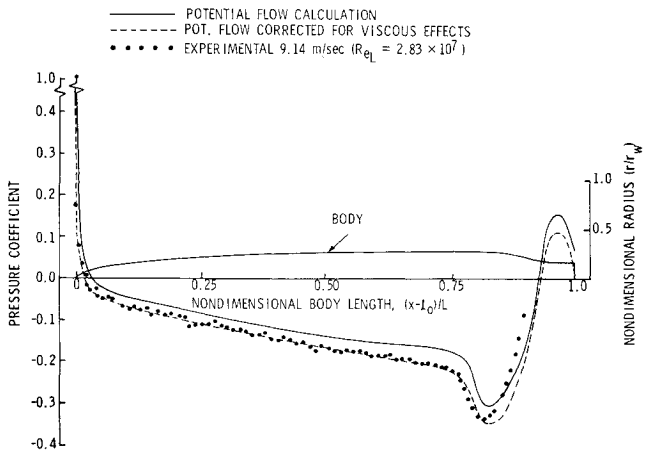

Fig. 6 Comparison of the in-tunnel potential flow and corrected potential flow pressure distributions with one determined experimentally at 9.14 m/s in the 1.22-m-diam water tunnel.

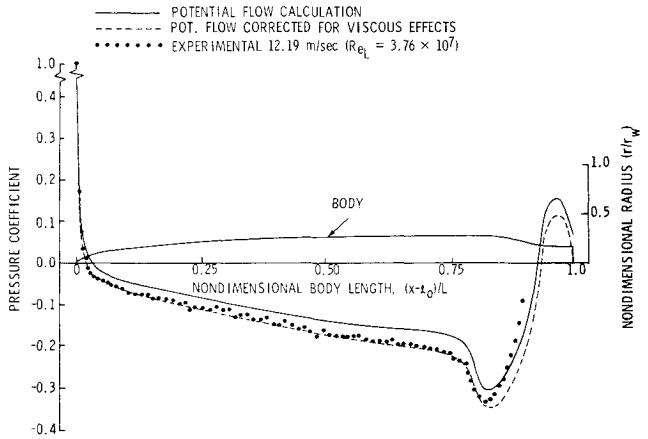

Fig. 7 Comparison of the in-tunnel potential flow and corrected potential flow pressure distributions with one determined experimentally at 12.19 m/s in the 1.22-m-diam water tunnel.

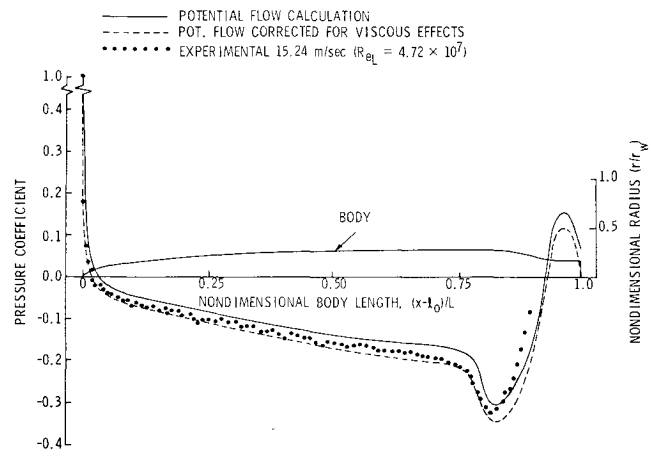

Fig. 8 Comparison of the in-tunnel potential flow and corrected potential flow pressure distributions with one determined experimentally at 15.24 m/s in the 1.22-m-diam water tunnel.

in this laminar flow regime. For $s>s_t$, τ_b is calculated according to Eq. (21) with the appropriate change from x to s variable. The integral in Eq. (18) is evaluated numerically using Simpson's rule.

The integrals of Eq. (20) are also evaluated using Simpson's rule. Both p_b and p_b' are determined from the body in a cylindrical duct Douglas-Neumann solution. In this numerical example, we calculated δ_b^* (needed to obtain p_b') using an axisymmetric, implicit finite-difference solution of the boundary-layer equations of motion.

Because of the thicker boundary layers, ΔCp is largest at the lower velocities. Thus, at 6.01 m/s, a few typical values of ΔCp_i ($i=1,2,3,4$) are presented in Table 2 from which an assessment of the contribution of each ΔCp_i to the total ΔCp can be made. Clearly, ΔCp_3 contributes the greatest to ΔCp, but ΔCp_1 and ΔCp_2 are also significant contributors. On the other hand, ΔCp_4 is approximately an order of magnitude lower than ΔCp_2 ($\Delta Cp_2<\Delta Cp_1<\Delta Cp_3$) for those locations on the body where the flow is turbulent. Obviously, ΔCp_4 is the most tedious to calculate, so it may be conveniently justified to neglect it entirely from the computations. For those conditions in which the computations are compared to experimental data, this deletion has been made. It is further noted that if body flow is entirely laminar, ΔCp_2 may also be neglected; although, we have retained it for all of the computations in this example because there is only a small regime of laminar flow on the body.

Figures 5-8 summarize the comparisons of potential flow, corrected potential flow, and experimental pressure distributions for our given body operating at 6.09-15.24 m/s

test-section velocities. At all speeds, the horizontal buoyancy correction theory agrees well with the experimental data, particularly for those body positions forward of Cp_{min}. Aft of Cp_{min} there is a region of strong interaction where coupling between the boundary-layer flow and the potential outer flow becomes important. The theory presented here is not applicable to this region.

Conclusions

The analysis presented here is applicable to many practical problems involving the flow about bodies of revolution within cylindrical ducts, such as wind- or water-tunnel test sections. In particular, this analysis allows one to correct an inviscid, in-duct body pressure distribution for the effects of horizontal buoyancy. The derived expressions are relatively simple; thus, computations are performed using very simple Fortran or desk-top calculator progams. Based on the experimental observations of, and on the computations performed for a particular body that operates in a given water tunnel test section, horizontal buoyancy effects were shown to be important and should not be neglected if precise pressure coefficient values are required. We have demonstrated that the theory adequately predicts the observed effects, except in the afterbody region where strong interaction effects dominate.

Acknowledgments

The author is indepted to B.R. Parkin, G.H. Hoffman, and R.E. Henderson for their suggestions regarding this investigation, and to M.E. Henderson for carrying out the calculations presented in the numerical example. He is especially indebted to G.B. Gurney for his assistance in the experimental portion of this investigation. This work has been supported by the U.S. Naval Sea Systems Command, Code 035.

References

[1] Hess, J.L. and Martin Jr., R.P., "Improved Solution for Potential Flow About Arbitrary Axisymmetric Bodies by the Use of a Higher Order Surface Source Method: Part I, Theory and Results," NASA CR 134694, MDC J6627-01, July 1974.

[2] Friedman, D.M., "Improved Solution for Potential Flow About Arbitrary Axisymmetric Bodies by the Use of a Higher-Order Surface Source Method: Part II. User's Manual for Computer Program," NASA CR 134695, MDC J6627-02, July 1974.

[3] Goodman, T.R., "Aerodynamic Characteristics of a Slender Body Traveling in a Tube," *AIAA Journal,* Vol. 9, April 1971, pp. 712-717.

[4] Landweber, L., "Axisymmetric Potential Flow in a Circular Tube," *Journal of Hydronautics,* Vol. 8, Oct. 1974, pp. 137-145.

[5] Varsamov, K. and Haimov, A., "Axisymmetric Potential Flow in Ducts," *Journal of Hydronautics,* Vol. 12, April 1978, pp. 78-80.

[6] Schlichting, H., *Boundary-Layer Theory,* 6th ed., McGraw-Hill Book Co., New York, 1968.

[7] Ross, D. and McGinley, J.H., "Flow in Closed-Jet Working Sections," Ordnance Research Laboratory External Rept. NOrd 7958-283, Feb. 1954, The Pennsylvania State University, Applied Research Laboratory.

[8] Lehman, A.F., "The Garfield Thomas Water Tunnel," Ordnance Research Laboratory External Rept. NOrd 16597-56, Sept. 1959, The Pennsylvania State University, Applied Research Laboratory.